Characterization of Hot Deformation Behavior of Brasses Using Processing Maps: Part II. β Brass and α-β Brass

D. PADMAVARDHANI AND Y.V.R.K. PRASAD

The hot deformation behaviors of β brass in the temperature range of 550 °C to 800 °C and α-β brass in the temperature range of 450 °C to 800 °C have been characterized in the strain rate range of 0.001 to 100 s^{-1} using processing maps developed on the basis of the Dynamic Materials Model. The map for β brass revealed a domain of superplasticity in the entire temperature range and at strain rates lower than 1 s^{-1}, with a maximum efficiency of power dissipation of about 68 pct. The temperature variation of the efficiency of power dissipation in the domain is similar to that of the diffusion coefficient for zinc in β brass, confirming that the diffusion-accommodated flow controls the superplasticity. The material undergoes microstructural instability in the form of adiabatic shear bands and strain markings at temperatures lower than 700 °C and at strain rates higher than 10 s^{-1}. The map for α-β brass revealed a wide domain for processing in the temperature range of 550 °C to 800 °C and at strain rates lower than 1 s^{-1}, with a maximum efficiency of 54 pct occurring at about 750 °C and 0.001 s^{-1}. In the domain, the α phase undergoes dynamic recrystallization and controls the hot deformation of the alloy, while the β phase deforms superplastically. At strain rates greater than 1 s^{-1}, α-β brass exhibits microstructural instabilities manifested as flow rotations at lower temperatures and localized shear bands at higher temperatures.

I. INTRODUCTION

A study of the hot deformation behavior of two-phase materials will be useful for processing commercial alloys since many of them have two or more phases. Alpha-beta brass is one such material where the α and β phases have different constitutive flow behaviors. Alpha brass exhibits[1] a dynamic recrystallization domain in the temperature range of 750 °C to 850 °C and at strain rates of 0.001 to 1 s^{-1}, while β brass undergoes superplastic deformation[2] under similar conditions. The aim of the present investigation is to examine the deformation behavior of α-β brass from the point of view of the influence of the constitutive behavior of the individual α and β phases. For this purpose, the approach of characterizing the hot deformation behavior using power dissipation maps will be adopted.

The maps are developed on the basis of the Dynamic Materials Model,[3] which was reviewed recently by Gegel *et al.*[4] and Alexander.[5] In this model, the workpiece material under hot working condition is considered to be a dissipator of power, and the instantaneous power dissipated at a given strain rate ($\dot{\varepsilon}$), temperature, and strain may be considered to consist of two parts: G content, representing the temperature rise, and J cocontent, representing the dissipation through metallurgical processes. The factor that partitions power between J and G is the strain rate sensitivity (m) of flow stress (σ), and the J cocontent is given by

$$J = \sigma\dot{\varepsilon}m/(m + 1) \qquad [1]$$

For an ideal linear dissipator, $J = J_{max} = \sigma\dot{\varepsilon}/2$, and the J cocontent may be normalized with respect to J_{max} to obtain a dimensionless parameter defined as efficiency of power dissipation, η, given by

$$\eta = 2m/(m + 1) \qquad [2]$$

The constitutive behavior of the workpiece material in terms of dissipative microstructural mechanisms may be represented through the efficiency variations as a function of temperature and strain rate to obtain a power dissipation map.

The power dissipation map for hot deformation of α brass was given earlier.[1] In this article, the processing map for β brass is given and the deformation behavior of α-β brass is discussed in terms of the constitutive behaviors of the individual phases.

Hot deformation studies on β brass are very limited. Griffiths and Hammond[2] observed superplastic deformation in β brass in the temperature range of 500 °C to 800 °C and at lower strain rates. Strain rate sensitivities reaching close to unity, typical of Newtonian flow, were also reported in this study. The high-temperature diffusion rates[6] are fast in this material and are responsible for the abnormal grain growth in β brass. Anomalous ductility was observed and interpreted in terms of the effect of phase transformations.[7] Deformation bands were reported at temperatures below 425 °C and under impact conditions.[8]

In α-β brass, the mechanism of hot deformation has been studied, particularly with respect to superplasticity.[9–13] Fine-grained microduplex α-β brass exhibited high elongations[9] at 625 °C and at strain rates of 5×10^{-4} s^{-1}, while at higher strain rates, extensive cavitation at intergranular and interphase boundaries occurred.[10,11] The effect of grain size and shape on the flow stress of 60-40 brass under superplastic conditions was also considered[12] important. Further, small additions of Ce were reported[13,14] to improve the ductility of α-β brass, mainly through a decrease in the volume

D. PADMAVARDHANI, Graduate Student, and Y.V.R.K. PRASAD, Professor, are with the Department of Metallurgy, Indian Institute of Science, Bangalore 560012, India.

Manuscript submitted January 17, 1991.

fraction of harder α phase. The constitutive flow behavior in α-β brass was studied,[15] taking into account the nature of deformation of the two individual phases. It was concluded that the behavior of the superplastic alloy resembles that of the softer β phase, while the harder α phase slides and rotates along interphase boundaries. Microstructural changes during hot deformation of α-β brass were investigated by Roberts and Otterberg.[16] At higher temperatures, the brass behaves as though it were wholely β, while at lower temperatures, dynamic recrystallization was observed. Hennaut *et al.*[17] examined the evolution of microstructure using optical microscopy and X-ray diffraction and concluded that dynamic recrystallization of α phase occurs at 680 °C, the degree of dynamic recrystallization being higher at lower strain rates.

II. EXPERIMENTAL

Beta brass having 43.8 pct Zn was used in the study. The starting material was in the form of hot-rolled rods (rolling temperature 750 °C) which had an average grain diameter of about 1 mm. The temperature range employed for deformation of β brass was 550 °C to 800 °C, and the strain rate range was 0.001 to 100 s^{-1}.

Commercial α-β brass with 39.5 pct Zn, 3 pct Pb, and the rest Cu was used in this investigation. The starting material was in the form of extruded rods, the microstructure of which is shown in Figure 1. The microstructure had a feathery appearance and directionality. The temperature range employed for deformation of α-β brass was 450 °C to 800 °C, and the strain rate range was 0.001 to 100 s^{-1}.

Cylindrical specimens of 10 mm in diameter and 15 mm in height were machined for hot compression testing such that the compression axis was parallel to the rolling or extrusion direction. The specimens had concentric grooves on their faces to facilitate the retention of the lubricant during compression, and the edges were given a 1-mm 45 deg chamfer to avoid foldover in the initial stages of compression. Molten glass lubricant at temperatures higher than 650 °C and molybdenum disulfide with graphite at lower temperatures were used as lubricants. Hot compression tests were conducted on a microprocessor-controlled servohydraulic testing machine (DARTEC, Stourbridge, West Midlands, United Kingdom) which has the facility for an exponential decay of actuator speed to give constant true strain rates during the test. The temperature of the specimen, as well as the adiabatic temperature rise during compression, was measured with the help of a thermocouple embedded in the specimen. The deformed specimens were water quenched (β brass) or air cooled (α-β brass), sectioned vertically, and prepared for metallographic examination using standard techniques.

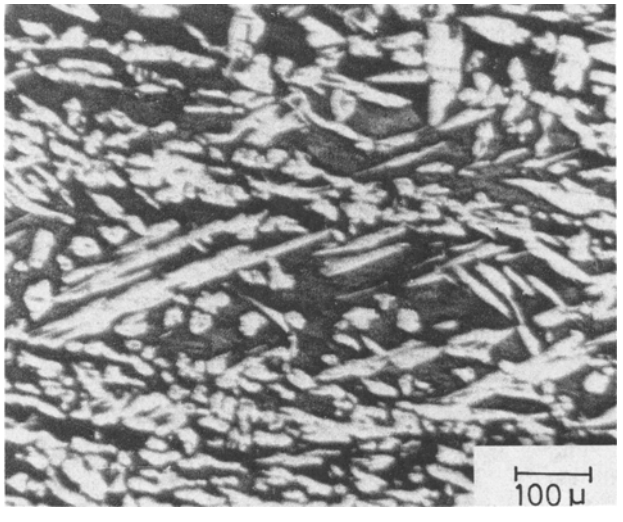

Fig. 1—Initial microstructure of α-β brass in the longitudinal direction showing feathery α phase.

The procedure for obtaining power dissipation maps was as follows. The load-stroke curves obtained in compression at a constant temperature and strain rate were converted into true stress-true plastic strain curves using standard equations. The flow stress data as a function of temperature, strain rate, and strain were obtained from the above curves and used for constructing the power dissipation maps.[3] The log flow stress *vs* log strain rate data were fitted using a cubic spline, and the strain rate sensitivity (m) was calculated as a function of strain rate. This was repeated at different temperatures. The efficiency of power dissipation through microstructural changes [$\eta = 2m/(m + 1)$] was then calculated as a function of temperature and strain rate and plotted as a three-dimensional (3-D) map and an isoefficiency contour map.

In addition to the power dissipation maps, maps predicting microstructural instabilities during flow were also developed on the basis of the flow stress data and using the continuum criterion developed by Kumar[18] on the basis of Zeigler's[19] principle of maximum rate of entropy production. It was shown that instabilities in microstructure will occur if

$$\xi(\dot{\varepsilon}) = (\partial \ln [m/(m + 1)]/(\partial \ln \dot{\varepsilon})) + m < 0 \quad [3]$$

The variation of $\xi(\dot{\varepsilon})$ with temperature and strain rate was plotted as an instability contour map showing regimes of unstable flow under conditions of negative $\xi(\dot{\varepsilon})$ values.

III. RESULTS AND DISCUSSION

A. *Beta Brass*

Typical true stress-true plastic strain curves recorded on β brass at 750 °C and at different strain rates are shown in Figure 2, which shows the following features:

(a) At strain rates of 1 s^{-1} and below, the stress-strain curves exhibited steady-state behavior.
(b) At higher strain rates (10 and 100 s^{-1}), the stress-strain curves exhibited oscillations.

The above trend is observed at all temperatures in the range studied (550 °C to 800 °C).

The flow stress data corrected for the adiabatic temperature rise are shown in Table I for β brass. The material exhibited low flow stresses at lower strain rates, particularly at high temperatures. The power dissipation

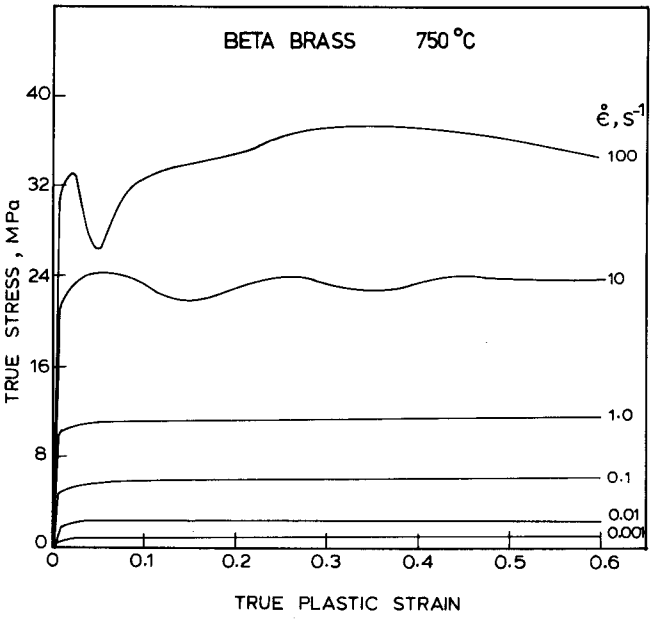

Fig. 2—True stress-true plastic strain curves for β brass at 750 °C and at various strain rates.

map for β brass is shown in Figure 3 for a strain of 0.3. Figure 3(a) is a 3-D view of the processing map, while Figure 3(b) is the corresponding isoefficiency representation. A comparison of the maps at different strains revealed that the characteristics are not changed appreciably with strain. The map exhibits a single domain, with an efficiency maximum of 68 pct occurring at about 800 °C and 0.001 s^{-1}. The domain extends up to a strain rate of 1 s^{-1} over the whole temperature range. The instability map developed on the basis of the continuum criterion given by Eq. [3] at a strain of 0.5 is shown in Figure 4. Instability is indicated at temperatures lower than 700 °C and at strain rates higher than 10 s^{-1}. It is in this regime that the stress-strain curves exhibit oscillations.

The basis for the interpretation of power dissipation maps in terms of microstructural processes is the Dynamic Materials Model.[3,4,5] According to Raj[20] maps, the high-temperature, low strain rate domain represents the process of wedge cracking. Under these conditions, grain boundary sliding occurs and causes stress concentration at grain boundary triple junctions, leading to wedge cracks. However, if the stress concentration is relieved by diffusion-accommodated flow, the extent of wedge

Table I. Flow Stress Values (in MPa) of β Brass at Different Strain Rates and Temperatures for Various Strains (Corrected for Adiabatic Temperature Rise)

Strain	Strain Rate (s^{-1})	Temperature (°C)					
		550	600	650	700	750	800
0.1	0.001	4.7	2.3	1.4	0.8	0.7	0.7
	0.010	9.3	5.7	4.3	2.9	2.4	2.6
	0.100	16.4	11.2	10.3	6.2	5.7	4.3
	1.000	34.9	24.3	19.1	14.5	11.4	9.0
	10.000	59.8	53.0	35.5	28.6	23.6	18.8
	100.000	80.2	61.8	48.4	40.5	32.8	27.5
0.2	0.001	4.4	2.6	1.6	0.9	0.8	0.7
	0.010	9.4	5.8	4.4	3.0	2.3	2.6
	0.100	16.4	11.6	10.4	6.8	5.9	4.7
	1.000	33.9	24.0	19.1	14.6	11.5	9.4
	10.000	60.0	52.3	35.4	29.4	23.5	18.6
	100.000	87.1	67.7	52.2	44.3	35.3	29.4
0.3	0.001	4.5	2.6	1.6	1.1	0.8	0.8
	0.010	9.5	5.7	4.5	3.2	2.4	2.8
	0.100	16.7	11.8	10.9	7.1	6.0	4.9
	1.000	33.6	24.7	19.6	14.9	11.5	9.5
	10.000	60.0	52.7	35.7	28.3	23.5	18.5
	100.000	89.6	71.7	55.1	46.6	37.6	31.7
0.4	0.001	4.7	2.9	1.7	1.2	0.9	0.8
	0.010	9.7	5.8	4.5	3.3	2.5	2.8
	0.100	16.7	12.2	11.1	7.5	6.1	4.9
	1.000	33.9	25.2	20.2	15.2	11.8	9.7
	10.000	60.4	52.2	36.8	29.8	23.9	19.1
	100.000	90.0	70.9	55.5	46.7	37.7	31.9
0.5	0.001	4.7	3.0	1.8	1.3	1.1	1.0
	0.010	9.7	6.0	4.6	3.3	2.5	3.0
	0.100	17.2	12.5	11.4	7.7	6.2	4.8
	1.000	34.2	25.7	20.6	15.3	12.0	9.8
	10.000	60.8	52.8	37.5	29.4	24.3	19.5
	100.000	86.9	68.6	53.8	45.8	36.8	31.3

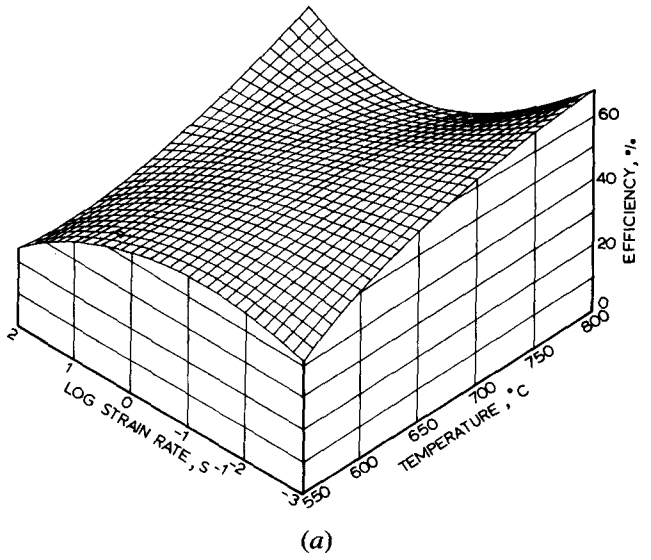

(a)

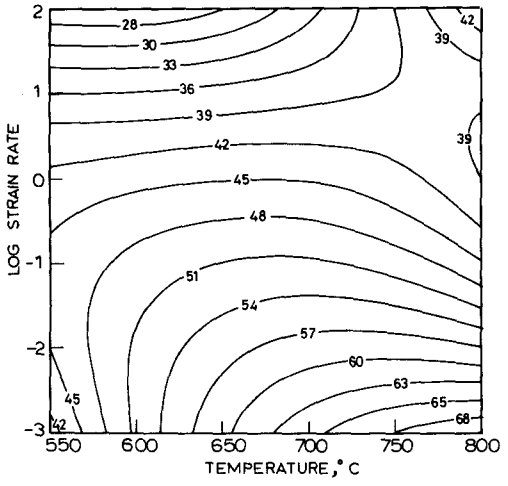

(b)

Fig. 3—(*a*) 3-D view of the power dissipation map for β brass at a strain of 0.3. (*b*) Contour map showing isoefficiency contours in strain rate-temperature plane for β brass at a strain of 0.3. The numbers indicate the efficiency of power dissipation in percent.

cracking may become less, resulting in extensive ductility. This is referred to as superplasticity,[21] which is characterized[2] by high strain rate sensitivities (>0.3), low flow stresses independent of strain, and high ductilities. In view of the high strain rate sensitivity, the efficiency of power dissipation for superplasticity is generally >50 pct and often reaches values close to 100 pct. For example, in fine-grained Ti-6Al-4V alloy, a domain with efficiency of 90 pct has been identified[22] to represent superplasticity which was characterized[23] extensively. Efficiency of 100 pct (strain rate sensitivity = 1) was reported[2] in β brass and interpreted as to represent Newtonian viscous flow. The map for β brass (Figure 3) exhibits a domain with a high efficiency of 68 pct and hence may be identified to represent superplastic deformation. Since diffusional flow plays a critical role in inducing superplasticity, the temperature dependence of the efficiency of power dissipation at low strain rates should be comparable to that of the diffusion coefficient. The variations of the efficiency of power dissipation at

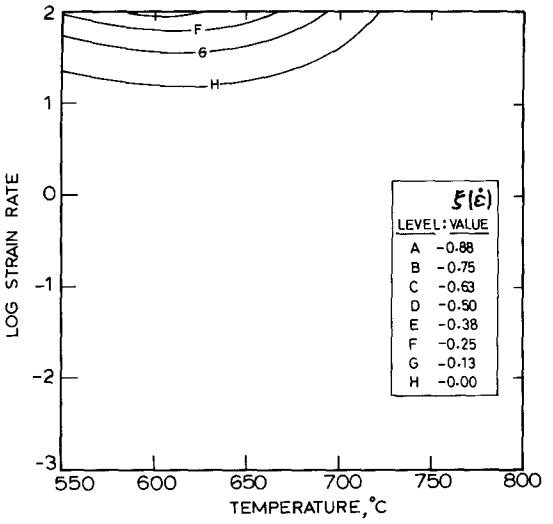

Fig. 4—Instability map showing contours of instability parameter $\xi(\dot{\varepsilon})$ in strain rate-temperature plane for β brass at a strain of 0.5. Instability is predicted when $\xi(\dot{\varepsilon})$ is negative.

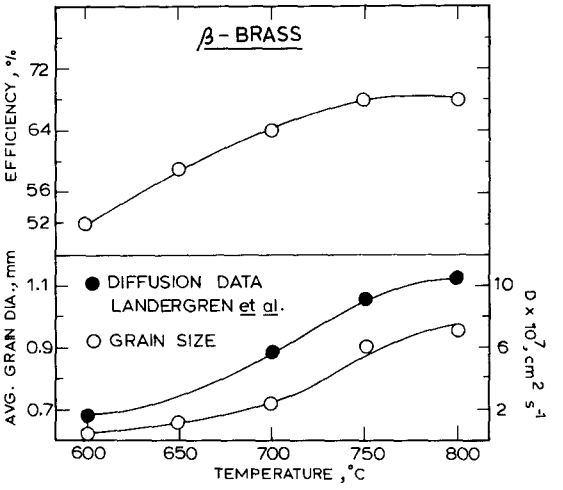

Fig. 5—Variation of efficiency of power dissipation at a strain rate of 0.001 s^{-1} and diffusion coefficient with temperature for β brass. The variation of the average grain diameter in the samples deformed at 0.001 s^{-1} is also shown.

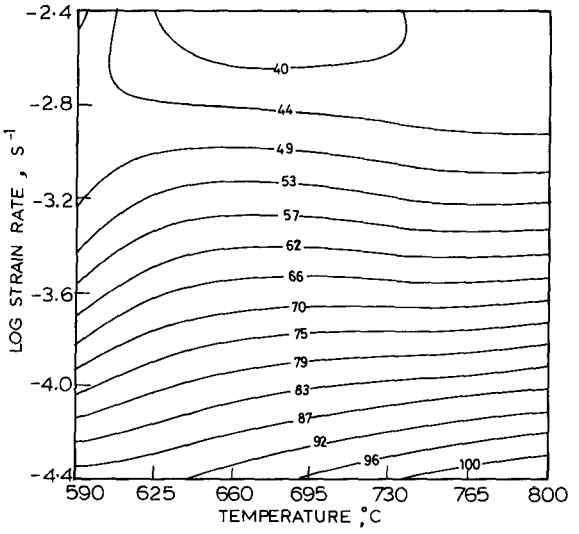

Fig. 6—Power dissipation map of β brass developed on the basis of the data of Griffiths and Hammond.[2]

0.001 s^{-1} and that of the diffusion coefficient[6] for different temperatures are shown in Figure 5. The striking similarity confirms that the domain represents superplasticity. The grain size variation of the samples deformed at 0.001 s^{-1} with temperature also follows a similar trend to that of the diffusion coefficient. In addition, the steady-state stress-strain curves and the high diffusion coefficients lend further support to the interpretation of the domain to represent superplasticity.

On the basis of the flow stress data at different temperatures and strain rates given by Griffiths and Hammond,[2] a processing map is developed and is shown in Figure 6. The map shows a wide superplasticity domain with efficiency reaching 100 pct. This also confirms that β brass undergoes superplastic deformation at high temperatures and low strain rates.

The continuum criterion given by Kumar[18] predicts

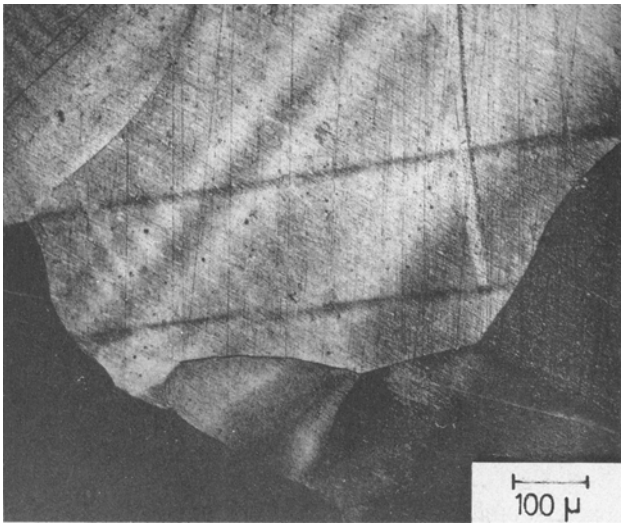

(*a*)

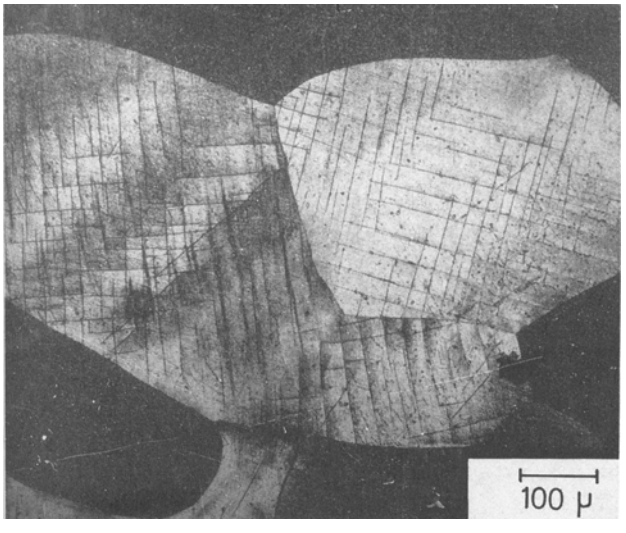

(*b*)

Fig. 7—Microstructure of the β brass specimen deformed at 650 °C and 10 s^{-1} (instability region) revealing (*a*) adiabatic shear bands and (*b*) strain markings.

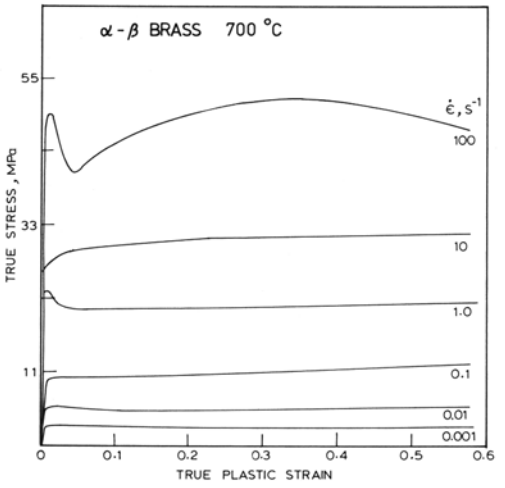

Fig. 8—True stress-true plastic strain curves for α-β brass at 700 °C and at various strain rates.

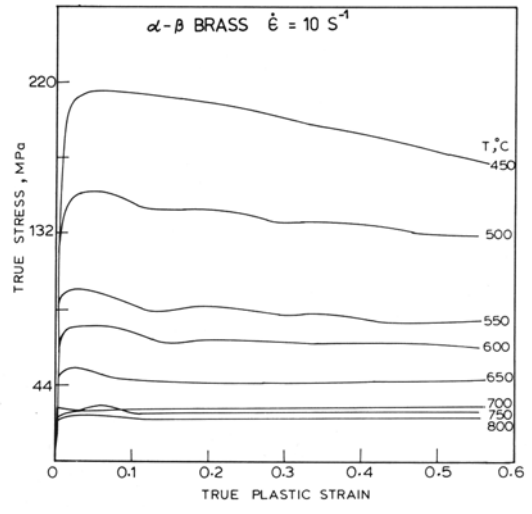

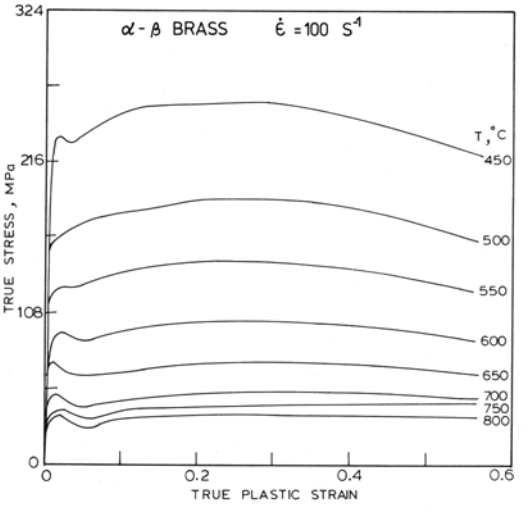

Fig. 9—True stress-true plastic strain curves for α-β brass at (*a*) 10 s^{-1} and (*b*) 100 s^{-1} and at various temperatures.

Table II. Flow Stress Values (in MPa) for α-β Brass at Different Strain Rates and Temperatures for Various Strains (Corrected for Adiabatic Temperature Rise)

Strain	Strain Rate (s^{-1})	Temperature (°C)							
		450	500	550	600	650	700	750	800
0.1	0.001	43.7	23.3	13.8	7.6	4.3	2.7	1.9	1.5
	0.010	58.0	35.5	24.1	14.8	8.6	5.4	3.7	4.3
	0.100	106.7	58.3	38.6	24.8	15.7	10.2	8.8	7.0
	1.000	178.6	101.7	72.5	43.1	28.5	21.0	16.0	15.2
	10.000	251.6	170.2	111.4	79.4	50.1	31.3	28.6	26.0
	100.000	276.5	204.4	155.6	105.5	67.3	46.4	38.2	32.3
0.2	0.001	39.6	21.7	12.4	6.8	3.9	2.5	1.9	1.5
	0.010	54.7	33.8	22.1	13.7	8.3	5.3	3.5	4.5
	0.100	99.2	55.6	36.8	23.8	15.6	10.4	9.0	6.4
	1.000	163.9	95.9	67.3	41.3	27.2	20.6	15.8	16.0
	10.000	245.7	166.1	109.7	75.9	48.0	31.8	28.7	24.9
	100.000	283.7	213.2	164.0	111.5	73.6	50.6	41.8	34.4
0.3	0.001	36.7	20.8	11.3	5.9	3.6	2.4	1.8	1.6
	0.010	52.8	33.0	20.9	13.3	8.0	5.4	3.5	4.5
	0.100	93.0	53.1	36.1	22.7	15.1	10.7	9.4	6.3
	1.000	153.3	90.9	65.6	40.2	26.9	20.9	15.9	16.6
	10.000	236.6	157.8	103.8	73.0	47.7	32.0	28.7	25.6
	100.000	285.0	214.7	164.2	113.3	75.7	53.4	43.9	36.2
0.4	0.001	34.3	20.1	10.9	5.2	3.4	2.5	1.9	1.6
	0.010	52.1	31.8	20.0	12.8	7.9	5.4	3.5	4.9
	0.100	88.9	52.7	35.3	22.2	15.2	11.3	9.6	6.4
	1.000	144.9	88.8	63.4	39.5	26.7	21.1	16.0	17.7
	10.000	221.8	153.6	101.5	72.1	48.1	32.2	28.8	25.3
	100.000	274.8	207.0	158.9	110.0	73.9	53.0	44.8	36.1
0.5	0.001	32.7	19.4	10.7	4.8	3.2	2.6	2.0	1.6
	0.010	51.1	31.2	19.8	12.4	7.8	5.7	3.5	5.1
	0.100	87.6	52.1	34.9	22.0	15.4	11.8	9.9	6.4
	1.000	140.0	86.8	62.9	39.1	26.5	21.4	16.1	19.1
	10.000	206.5	146.7	98.7	70.9	48.6	32.5	28.9	25.4
	100.000	257.9	193.3	148.1	103.4	70.1	50.8	44.5	35.4

that microstructural instabilities occur at lower temperatures and higher strain rates. The stress-strain behavior shows that oscillations appear in the flow curves. Microstructural investigations of the specimens deformed in the instability regime (550 °C to 700 °C and 10 to 100 s^{-1}) have revealed that the manifestation of the instability is in the form of adiabatic shear bands and strain markings (Figures 7(a) and (b)). They disappear when the strain rate is reduced or when the temperature is increased beyond 700 °C.

B. α-β *Brass*

Typical stress-strain curves of the specimens deformed at 700 °C at different strain rates are shown in Figure 8. The stress-strain curves at strain rates less than or equal to 0.1 s^{-1} exhibited steady-state behavior, while those at higher strain rates showed peculiar shapes (Figures 9(a) and (b)). The flow stress values corrected for adiabatic temperature rise at different temperatures and strain rates are given in Table II.

The processing map developed on the basis of the above data is shown in Figure 10 at a strain of 0.3. Figure 10(a) is the 3-D view, and Figure 10(b) is the isoefficiency contour representation of it. A comparison of the maps obtained at different strains showed that the general features essentially remained unchanged with strain. Referring to Figure 10, the processing map exhibits a wide domain in the temperature range of 550 °C to 800 °C and at strain rates lower than 1 s^{-1}, with a maximum efficiency of 54 pct occurring at 750 °C and 0.001 s^{-1}.

The instability map developed on the basis of the continuum criterion given by Eq. [3] is shown in Figure 11 for a strain of 0.5. The map reveals that the material undergoes microstructural instability when deformed at strain rates higher than 1 s^{-1}. The instability is intense at the lower (450 °C) and at the higher (800 °C) temperatures and at 100 s^{-1}.

The two phases that constitute α-β brass have entirely different constitutive flow behaviors under hot working conditions. At high temperatures and low strain rates, α undergoes dynamic recrystallization with a maximum efficiency of 54 pct, while β undergoes superplastic deformation with a maximum efficiency of 68 pct. Both the materials undergo microstructural instabilities at high strain rates and exhibit oscillations in the stress-strain curves.

On the basis of the above results, the processing map of α-β brass (Figure 10) may be interpreted as follows. The domain observed between 550 °C and 800 °C and at strain rates lower than 1 s^{-1} represents the dynamic recrystallization of the α phase, since the efficiency

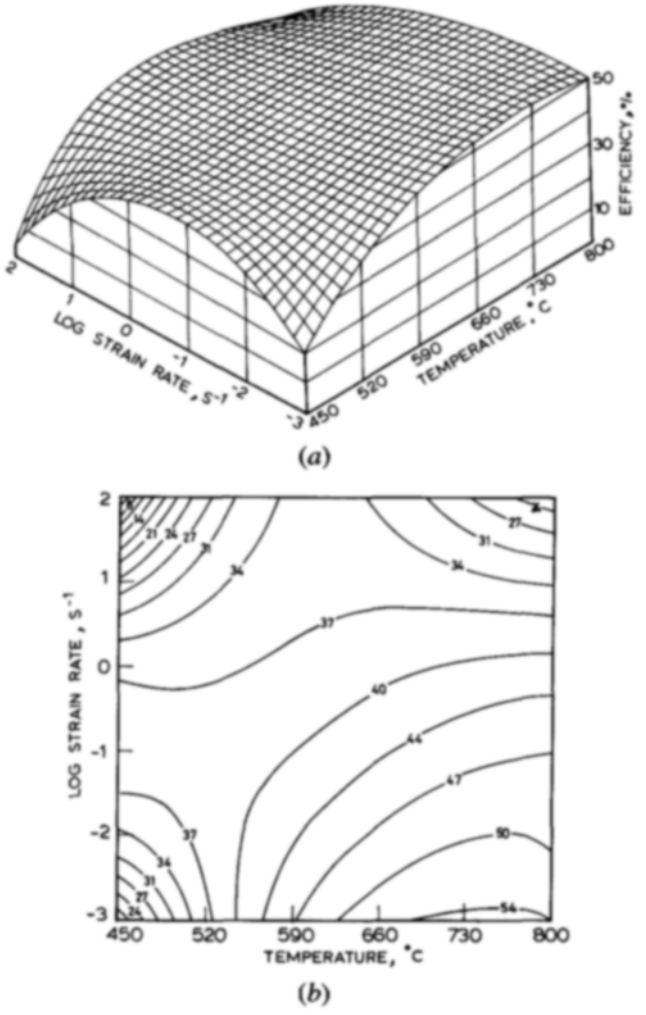

Fig. 10—(*a*) 3-D view of the power dissipation map for α-β brass at a strain of 0.3. (*b*) Contour map showing isoefficiency contours in strain rate-temperature plane for α-β brass at a strain of 0.3. The numbers indicate the efficiency of power dissipation in percent.

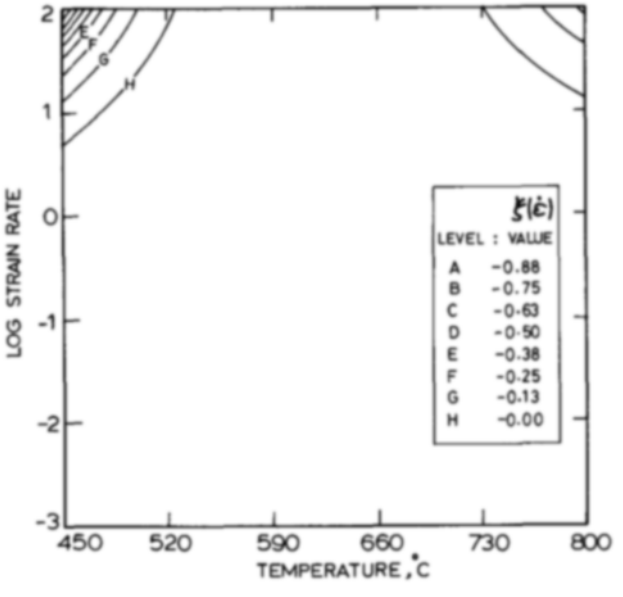

Fig. 11—Instability map showing contours of instability parameter $\xi(\dot{\varepsilon})$ in strain rate-temperature plane for α-β brass at a strain of 0.5. Instability is predicted when $\xi(\dot{\varepsilon})$ is negative.

matches with that observed in α brass (54 pct). The regime where solute drag effects are present in α brass (650 °C and 0.001 s^{-1}) is shifted to lower temperatures in α-β brass (450 °C). This is expected, since the higher zinc content has a tendency to decrease the temperature for the onset of solute drag effects.[24] The β phase in the domain (550 °C to 800 °C and strain rates lower than 1 s^{-1}) undergoes superplastic deformation which is controlled by the diffusion of zinc in β phase. The activation energy[25] for the diffusion of zinc in β brass (70 kJ/mol) is much lower than that for the diffusion of zinc in α brass (168 kJ/mol), which controls the dynamic recrystallization of α brass. In view of this and the lower flow stresses for β at elevated temperatures, the deformation of β phase in α-β brass does not require any additional energy. Thus, the domain in α-β brass is interpreted to represent the dynamic recrystallization of α phase and

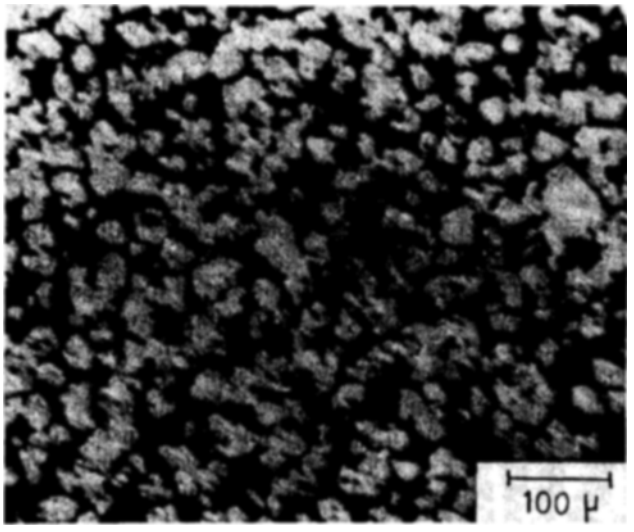

(*a*)

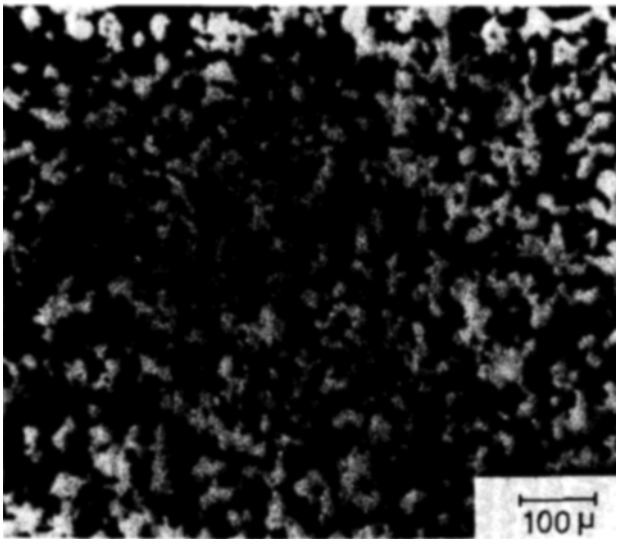

(*b*)

Fig. 12—Microstructure of the α-β brass specimen deformed at (*a*) 650 °C and 0.001 s^{-1} and (*b*) 650 °C and 0.01 s^{-1}, showing globularized α phase.

the superplastic deformation of β phase. The hot deformation behavior of the two-phase alloy is controlled by the dynamic recrystallization of α phase. The metallographic and X-ray diffraction studies of Hennaut *et al.*[17] are in support of this conclusion.

The microstructure of the sample deformed in the domain is shown in Figure 12(a). In comparison with the initial microstructure (Figure 1), a large-scale reconstitution of the α-phase morphology is seen. The α phase, which was feathery initially, is globularized after deformation. This confirms that the α phase has undergone dynamic recrystallization. At a higher strain rate in the domain (0.01 s^{-1}), similar dynamic recrystallization of α phase occurred with a phase refinement (Figure 12(b)). Away from the domain, at lower temperatures and strain rates (500 °C and 0.001 s^{-1}), the microstructure of the sample has not undergone significant change in the morphology of the α phase (Figure 13), which suggests dynamic recovery of α phase.

At high strain rates, the material undergoes microstructural instabilities predicted by the instability criterion[18] (Figure 11). The manifestations of these instabilities are dependent on the temperature of deformation. For example, at lower temperatures (450 °C and 100 s^{-1}), the manifestation is in the form of rotations (Figure 14(a)) with respect to the axis of compression. On the other hand, at high temperatures (800 °C and 100 s^{-1}), instability bands representing localized flow (Figure 14(b)) are seen, and these bands are oriented at an angle of about 35 deg with respect to the stress axis. From the instability map of the α phase given earlier[1] and that of β brass (Figure 4), it is seen that both the phases undergo instabilities at lower temperatures and high strain rates, while the β instability continues to higher temperatures. Thus, the low-temperature instability in α-β brass involves both the phases, while the higher temperature instability is due to the β phase only. These microstructural instabilities are responsible for the oscillations and unusual shapes of the stress-strain curves (Figure 9).

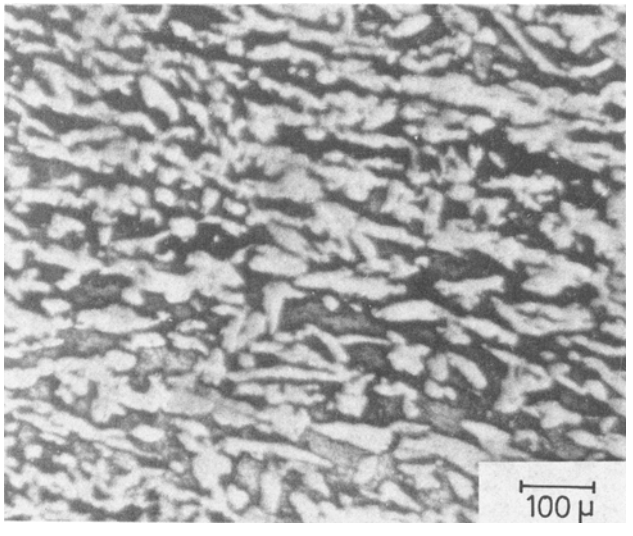

Fig. 13—Microstructure of the α-β brass specimen deformed at 500 °C and 0.001 s^{-1} showing no significant change in the morphology of the α phase.

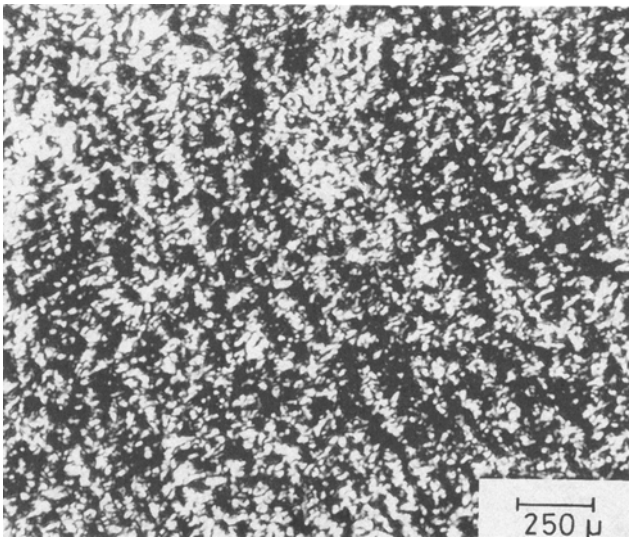

(*a*)

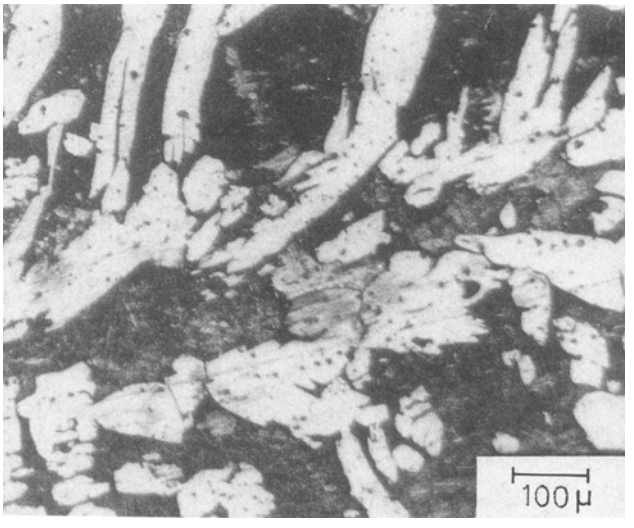

(*b*)

Fig. 14—(*a*) Microstructure of the α-β brass specimen deformed at 450 °C and 100 s^{-1} (instability region) revealing rotations and (*b*) 800 °C and 100 s^{-1} (instability region) revealing localized shear bands.

The behavior of microduplex α-β brass was shown[15] to be controlled by the β-phase deformation. In this microduplex structure, the sliding of the α-β interfaces dominates the hot deformation. The α-phase deformation is negligible under these conditions, since the power transfer does not occur across the α-β interface. Thus, the α phase in this case does not undergo dynamic recrystallization. The processing map for such a microduplex structure will show a domain of superplasticity with higher efficiencies. In contrast, the feathery microstructure of the two-phase alloy does not permit extensive sliding of the α-β interface and hence will transfer the power across the interface, leading to the dynamic recrystallization of α.

The studies on α-β brass by Roberts and Otterberg[16] showed flow softening at lower temperatures and higher strain rates and are interpreted in terms of dynamic recrystallization of α phase. However, the processing map and the instability map (Figures 10 and 11) indicate that under these conditions, the material is only marginally stable. Actual dynamic recrystallization of α phase occurs at lower strain rates. The microstructures presented in the study, even under these conditions of marginal stability, clearly showed the reconstitution of the microstructure, indicating a contribution from the dynamic recrystallization of α phase.

IV. CONCLUSIONS

The following conclusions are drawn from the study of the hot deformation behavior of β brass and α-β brass using the approach of processing maps in the strain rate range of 0.001 to 100 s^{-1} and the temperature range of 550 °C to 800 °C for β brass and 450 °C to 800 °C for α-β brass:

1. Beta brass undergoes superplastic deformation in the entire temperature range and at strain rates lower than 1 s^{-1}, and the maximum efficiency of power dissipation observed in the domain is 68 pct.
2. The superplastic deformation in β brass is controlled by the diffusion of zinc in β brass.
3. Beta brass undergoes microstructural instabilities in the temperature range of 550 °C to 700 °C and at strain rates higher than 10 s^{-1}, the manifestation being in the form of adiabatic shear bands and strain markings.
4. Alpha-beta brass exhibits a wide domain for processing in the temperature range of 550 °C to 800 °C and at strain rates lower than 1 s^{-1}, with a maximum efficiency of 54 pct occurring at about 750 °C and 0.001 s^{-1}. The hot workability is optimum under these conditions.
5. In this domain, the α phase undergoes dynamic recrystallization and controls the deformation of α-β brass, while the β phase undergoes superplastic deformation.
6. At higher strain rates, the material undergoes microstructural instabilities manifested as rotations at low temperatures and localized shear bands at high temperatures.

REFERENCES

1. D. Padmavardhani and Y.V.R.K. Prasad: *Metall. Trans. A*, 1991, vol. 22A, pp. 2985-92.
2. P. Griffiths and C. Hammond: *Acta Metall.*, 1972, vol. 20, pp. 935-45.
3. Y.V.R.K. Prasad, H.L. Gegel, S.M. Doraivelu, J.C. Malas, J.T. Morgan, K.A. Lark, and D.R. Barker: *Metall. Trans. A*, 1984, vol. 15A, pp. 1883-92.
4. H.L. Gegel, J.C. Malas, S.M. Doraivelu, and V.A. Shende: *Metals Handbook*, 9th ed., ASM INTERNATIONAL, Metals Park, OH, 1987, vol. 14, pp. 417-38.
5. J.M. Alexander: in *Modelling of Hot Deformation of Steels*, J.G. Lenard, ed., Springer-Verlag, Berlin, 1989, pp. 101-15.
6. U.S. Landergren, C.E. Birchenall, and R.F. Mehl: *J. Met.*, 1956, vol. 8, pp. 73-78.
7. A.A. Presnyakov and G.V. Starikova: *Fiz. Metal. Metalloved.*, 1961, vol. 12, pp. 873-78.
8. C.S. Barrett: *J. Met.*, 1954, vol. 6, pp. 1003-08.
9. S. Sagat, P. Blenkinsop, and D.M.R. Taplin: *J. Inst. Met.*, 1972, vol. 100, pp. 268-74.
10. T. Chandra, J.J. Jonas, and D.M.R. Taplin: *J. Mater. Sci.*, 1978, vol. 13, pp. 2380-84.
11. C.W. Humphries and N. Ridely: *J. Mater. Sci.*, 1978, vol. 13, pp. 2477-82.
12. M. Suery and B. Baudelet: *J. Mater. Sci.*, 1973, vol. 8, pp. 363-69.
13. D.M.R. Taplin and D. Chandra: *J. Mater. Sci.*, 1975, vol. 10, pp. 1642-43.
14. T. Chandra, J.J. Jonas, and D.M.R. Taplin: *J. Mater. Sci.*, 1976, vol. 11, pp. 1843-48.
15. M. Suery and B. Baudelet: *Phil. Mag. A*, 1980, vol. 41, pp. 41-64.
16. W. Roberts and R. Otterberg: *Microstructure Evolution in Association with Hot Working of a Dezincification-Resistant α/β Brass*, Swedish Institute of Metals Research Report No. 1362, Stockholm, 1979; *also see* W. Roberts: In *Deformation Processing and Structure*, G. Krauss, ed., ASM, Metals Park, OH, 1984, pp. 109-84.
17. Jacqueline Hennaut, Jacqueline Othmazouri, and Jacques Charlier: *Z. Metallkd.*, 1984, vol. 75, pp. 667-72.
18. A.K.S. Kalyan Kumar: M.Sc.(Engg.) Thesis, Indian Institute of Science, Bangalore, India, 1987.
19. H. Ziegler: in *Progress in Solid Mechanics*, I.N. Sneddon and R. Hill, eds., North-Holland Publishing Co., Amsterdam, The Netherlands, 1963, pp. 93-193.
20. R. Raj: *Metall. Trans. A*, 1981, vol. 12A, pp. 1089-97.
21. M.F. Ashby and R.A. Verall: *Acta Metall.*, 1973, vol. 21, pp. 149-63.
22. Y.V.R.K. Prasad, H.L. Gegel, J.T. Morgan, J.C. Malas, S.M. Doraivelu, and D.R. Barker: in *Titanium Net Shape Technologies*, F.H. Froes and D. Eylon, eds., TMS-AIME, Warrendale, PA, 1984, pp. 279-89.
23. S.M.L. Sastry, R.L. Lederich, T.C. Mackay, and W.R. Kerr: *J. Met.*, 1983, vol. 35, p. 48.
24. M. Mayer, D. Vohringer, and E. Macherauch: in *Strength of Metals and Alloys*, ICSMA 5, P. Haasen, V. Gerold, and G. Kostorz, eds., Pergamon Press, New York, NY, 1979, vol. 2, pp. 807-12.
25. T. Chandra, J.J. Jonas, and D.M.R. Taplin: *Z. Metallkd.*, 1977, vol. 68, pp. 546-49.